Looking for sp2carbon atoms in diamond: a quantum mechanical study of interacting vacancies

Looking for sp^2 Carbon Atoms in Diamond: a Quantum Mechanical Study of Interacting Vacancies.

Giuseppe Sansone,[1] Simone Salustro,[1] Yves Noël,[2] Lorenzo Maschio,[1] William C. Mackrodt,[1] and Roberto Dovesi[1]

[1]*Dipartimento di Chimica, Università di Torino and NIS (Nanostructured Interfaces and Surfaces) Centre, Via P. Giuria 5, 10125 Torino, Italy*

[2]*Institut des Sciences de la Terre de Paris (UMR 7193 UPMC-CNRS), UPMC, Sorbonne Universités, Paris, France*

(Dated: December 25, 2017)

This paper reports the calculated relaxed lattice configurations and corresponding electronic and magnetic structures, and Raman frequencies of two divacancies in diamond, V_2 and VC=CV, in which the vacancies are first and third neighbours respectively. The calculations are formulated within a supercell approach to local defects in crystalline solids, here 64- and 128-atoms unit cells and based largely on the B3LYP one-electron approximation constructed from an all-electron Gaussian basis set. Three important findings are first, that, of the four possible spin states, S_z=0, 1, 2, 3, the singlet is predicted to be lowest in energy for both divacancies; second, that the singlet state of V_2 is ∼1.7 eV lower in energy than that in VC=CV; and third, that the Raman peak at 1628 cm^{-1} in defective diamond can be ascribed to the presence of a C=C double bond, as in the singlet state of VC=CV.

I. INTRODUCTION

There has been long-standing theoretical[1–5] and experimental[6–9] interest in both native and radiation-induced defects in semiconductors. Of these, diamond, with a wide band gap, high Young's modulus, thermal conductivity and carrier mobility, and broad transparency range, has found widespread application in areas as diverse as micromechanical systems, heat sinks, laser windows and particle detectors.[10,11] However, it is known that the presence of defects can have a dramatic effect on its structural[12], optical[13] and electronic[14] properties. Clearly, then, both from a technological point of view, and diamond science more generally, an accurate, quantitative understanding of defects, which to some extent are always present, is important, not least in the interpretation of the plethora of often confusing and contradictory experimental data.[15–20] Of many experimental techniques that might be used to study diamond, and the more stable allotrope, graphite, vibrational spectroscopy, both infra-red and Raman, has been found to be particularly useful, for the different bonding in these systems, viz., sp^3 and sp^2 respectively, leads to characteristic vibrational frequencies, so that the presence of sp^2 electrons associated with vacancies in diamond, for example, might be detectable in this way. Consequently, vibrational spectroscopy has emerged as an important, further technique in the investigation of defect formation in irradiated diamond.[15,16,20–28]

The Raman spectrum of pristine diamond consists of a single, sharp peak at 1332 cm^{-1} corresponding to the first-order scattering of triply-degenerate TO(X) phonons of t_{2g} symmetry.[29] The irradiation-damaged crystal, on the other hand, exhibits several additional features which have been attributed to a variety of defects containing sp^2 and sp^3 electronic configurations. The most prominent of these to higher frequency than the first order line are located at about 1450, 1490, 1630 and 1680 cm^{-1}. The latter two have commonly been attributed to defects such as the "dumb-bell" split-interstitial containing sp^2 electrons[15,23], while the peaks at 1450 and 1490 cm^{-1} have variously been attributed to both vacancy and carbon/nitrogen interstitial defects.[30,31] Moreover, the first-order Raman peak is both broadened and red-shifted in damaged crystals.[23,27,30,31] This can tentatively be explained by noting that the peak frequency in pristine material depends primarily on the C-C bond length (and strength), and that if the former is increased in the damaged crystal, this would lead to a red-shift, *i.e.* lowering, of the original Raman frequency.

As a result of recent theoretical developments[32] and computational implementation of fully-analytic quantum mechanical methods for the *ab initio* evaluation of infra-red and Raman spectra in solids[32–35], computational vibrational spectroscopy is now established as an additional and effective tool in the interpretation of experimental spectra.[36–38] Accordingly, as a first step towards a more complete quantitative understanding of defective diamond, this paper reports the computed Raman spectra of the two lowest spin states of two neutral divacancies, V_2 and VC=CV, in which the vacancies are first and third neighbours (as reported in Figure 1), each at concentrations of (1/64) and (1/128) defects per carbon. These are compared to previous experimental and theoretical data.[39]

II. COMPUTATIONAL DETAILS

The calculations reported here are of two types: the first involves the quantum mechanical determination of the optimum, *i.e.* energy-minimised, lattice structure (atomic positions), total energy and electronic and spin structures of both perfect and defective diamond lattices based on periodic supercells; the second is the calculation of the phonon spectra, and from these the Raman active frequencies and intensities of the previously cal-

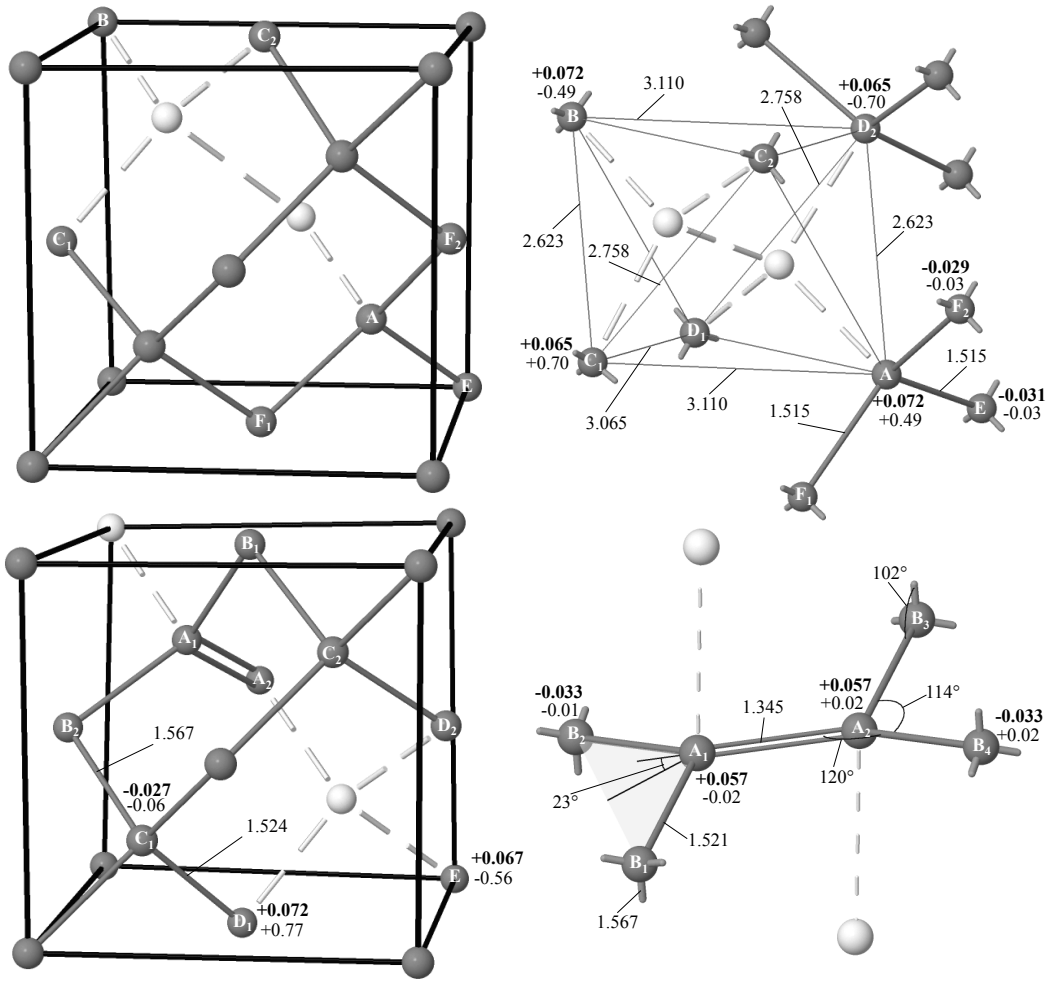

FIG. 1: B3LYP equilibrium geometries, net Mulliken charges and spin moments for the divacancies, V_2 (upper right) and VC=CV (lower right) based on S_{64}, where interatomic distances (normal) are in Å and angles in degrees. The equivalent conventional diamond cells are shown on the left, where atomic Mulliken net charges (bold) and spin moments (normal) are in $|e|$. White spheres represent vacancies, and dashed white lines their nearest neighbour connectivity.

culated structures and energy/displacement derivatives using recently implemented methods for calculating the infra-red and Raman spectra of solids.[32–35] In order to simulate the presence of vacancies in both defective structures, a complete removal of the atoms of interest (nuclei, electrons, basis set) has been performed. The majority of electronic structures and energies were obtained from the well-established B3LYP[40,41] hybrid implementation of density functional theory (DFT) in both spin un-polarised and unrestricted spin polarised descriptions using the CRYSTAL code.[32] The B3LYP approximation has been shown to give vibrational properties of solids that are comparable to, and in some cases superior to, those from other functionals.[37,38,42] An important feature of both the vacancies examined here is that they contain six unbound sp^3 electrons, which can give rise to four spin states, $\{\alpha\alpha\alpha\beta\beta\beta\}_{S_z=0}$, $\{\alpha\alpha\alpha\alpha\beta\beta\}_{S_z=1}$, $\{\alpha\alpha\alpha\alpha\alpha\beta\}_{S_z=2}$ and $\{\alpha\alpha\alpha\alpha\alpha\alpha\}_{S_z=3}$, for which we have used spin unrestricted hybrid DFT. Previous calculations for a diversity of open-shell systems[43–47] have shown that despite the evident deficiency with respect to S^2, but not S_z, this approach leads to acceptable, often accurate, descriptions of the magnetism. The use of 64- and 128-unit supercells, S_{64} and S_{128}, serves the twin purposes of investigating whether the vacancies are essentially isolated at these defect concentrations, and if not, the extent of the interaction. Crucial to the reliable prediction of formation energies and Raman frequencies, is the accurate calculation of the equilibrium structures of the defective crystal. To achieve this, the lattice parameters and *all* atomic positions of both the S_{64} and S_{128} unit cells have been optimised to a root mean square (r.m.s.) displacement of 10^{-5} Å. For the limited purposes of checking the formation energies of the two divacancies, PBE0[48] and HSE06[49] hybrid functionals have also been explored, in addition to the unscreened HF approximation and the

inclusion of Grimme's empirical dispersion correction[50] to the B3LYP potential.

In keeping with the use of the B3LYP, PBE0 and HSE06 functionals in their "standard" form, *i.e.* without any empirical adjustments in respect of the calculated Raman frequencies, Pople's (standard) 6-21G Gaussian basis set[51] has been adopted for the Bloch function expansions, except for the exponent of the most diffuse *sp* shell, which has been re-optimised (0.228 Bohr^{-2}) to minimise the energy of non-defective bulk diamond. Again, to check the divacancy formation energies, B3LYP calculations have also been carried out using 6-21G*, 6-31G and 6-31G* basis sets[52]; and for comparisons with previous reports, the PBE gradient corrected[53] and uncorrected LDA functionals[54] have also been examined. The computational parameters used in this report comprise five values (T_1–T_5) that control the truncation of the (infinite) Coulomb and exchange series[32], here set to 10^{-8} (T_1–T_4) and 10^{-16} (T_5); the SCF energy convergence threshold, which in this study was set to 10^{-8} Ha for structural optimisation and 10^{-10} Ha for the vibration frequency calculations; and the shrinking factors that control the number of independent **k**-points used in the sampling of the Monkhorst-Pack[55] net, here 150 and 24 points for S_{64} and S_{128} respectively.

For the lattice dynamics calculations, harmonic phonon frequencies, ω_p, were evaluated at the Γ point and obtained from the diagonalization of the mass-weighted Hessian matrix (second energy derivatives with respect to atomic displacements u[36,56,57])

$$W^{\Gamma}_{ai,bj} = \frac{H^{\mathbf{0}}_{ai,bj}}{\sqrt{M_a M_b}} \quad \text{with} \quad H^{\mathbf{0}}_{ai,bj} = \left(\frac{\partial^2 E}{\partial u^{\mathbf{0}}_{ai} \partial u^{\mathbf{0}}_{bj}} \right) , \quad (1)$$

where atoms a and b (with atomic masses M_a and M_b) in the reference cell, **0**, are displaced along the i-th and j-th Cartesian directions, respectively. First order derivatives were computed analytically, whereas second order derivatives were obtained numerically, using a two-point formula. The Raman intensity, $I^p_{ii'}$, corresponding to the Stokes' line of a phonon mode Q_p, can be expressed as

$$I^p_{ii'} \propto \left(\frac{\partial \alpha_{ii'}}{\partial Q_p} \right)^2 , \quad (2)$$

where $\alpha_{ii'}$ is the ii'^{th} component of the polarizability tensor $\boldsymbol{\alpha}$. Here the relative values of these intensities were computed analytically using a procedure recently implemented in the CRYSTAL code.[34,35]

III. RESULTS

A. Equilibrium structure, relative energies and electronic structure

Except where explicitly cited, the results reported in this section refer to B3LYP calculations, and energies, to the optimised (equilibrium) structures. Despite the evident differences between the local lattice structures surrounding V_2 and VC=CV, the spin configurations of the lowest energy states were found to be identical, which greatly facilitates comparisons between the two. Preliminary calculations ruled out S_z=2 on energy grounds, leaving the singlet, triplet and septet states for detailed examination. In the singlet state, the spins align $\{\alpha\alpha\beta\}$ on the three surrounding atoms of one vacancy, and $\{\alpha\beta\beta\}$ around the other; whereas in the triplet state, the spin alignment is either $\{\alpha\alpha\beta\}$ or $\{\alpha\beta\beta\}$ around *both* vacancies. There is just one septet alignment. The relative stability, ΔE, of the three lowest energy spin states of V_2 and VC=CV based on S_{64} and S_{128} are listed in Table I. The singlet state is found to be the most stable for both divacancies, with the triplet state slightly less stable, by (2.1 - 2.2) meV and (2.5 - 3.1) meV respectively for V_2 and VC=CV. The septet state is a further (60-80) meV higher in energy. For the isolated vacancy, the singlet-triplet difference[44] is approximately twice the divacancy values. Hyde-Volpe *et al.*[39] have reported a similar order of stability based on BLYP cluster calculations, with a difference of ∼8 meV between the singlet and triplet for the two divacancies, which is roughly three times that obtained here.

TABLE I: B3LYP relative stability, ΔE, and formation energy, E_f, for different spin states of V_2 and VC=CV based on S_{64} and S_{128}. Also given are $2\times E_f$ for the isolated vacancy.

	S_z	ΔE_{64}	E^f_{64}	ΔE_{128}	E^f_{128}
VC=CV	0	-	11.67	-	11.70
	1	0.068	11.74	0.084	11.78
	3	1.741	13.41	1.758	13.46
V_2	0	-	9.94	-	9.96
	1	0.060	9.99	0.057	10.01
	3	2.152	12.09	2.144	12.10
V_1	0	-	13.50	-	13.50
	1	0.217	13.94	0.223	13.94
	2	1.423	16.34	1.426	16.34

The formation energy of a defect is commonly given by,

$$E_f = E_P - E_D - nE_A \quad (3)$$

where E_P and E_D are the total energies of the pristine and defective diamond supercells, respectively, E_A is the energy *per atom* in bulk diamond and n is the number of vacancies in the unit cell, here 2. For comparison, the energies of the isolated vacancy are doubled. The values of E_f given in Table I show quite clearly that V_2 is more stable than VC=CV for all three spin states, with differences in energy varying from ∼1.7 eV for the singlet and triplet states to ∼1.3 eV for the septet. Table I also indicates that the association, or binding energy of two (isolated) S_z=0 vacancies to form a singlet V_2 is ∼-3.5 eV.

To examine the effects of basis sets of higher quality than Pople's 6-21G, the formation energies, E_f, of singlet V_2

and VC=CV were calculated using 6-21G, 6-21G^{opt}, 6-21G*, 6-31 and 6-31* basis sets, where 6-21G^{opt} contains the optimised outer *sp* exponent. These are given in Table II which shows that for the singlet state of both V_2 and VC=CV the maximum deviation from the 6-21G^{opt} value of E_f is 1.6%, while the average difference in E_f between the two divacancy values for the richer bases, 1.7 eV, is identical to the 6-21G^{opt} value. Changes in hybrid functional have also been examined. Table III contains singlet formation energies of V_2 and VC=CV based on LDA, UHF and four other hybrid approximations based on S_{64}. Also included are values reported by Hyde-Volpe *et al.*[39] based on both cluster and periodic supercell calculations. Once again, of prime concern is the variation in the formation energies of singlet V_2 and VC=CV with changes in exchange-correlation functional, and the differences between the two divacancies. As observed, UHF estimates for E_f deviate most from the B3LYP values, with decreases of 12% and 8% for V_2 and VC=CV respectively, although the difference between the two formation energies, 1.9 eV, remains much the same (1.7 eV). For both vacancies, the average of the alternative functional values for E_f, 9.86 eV and 11.79 eV, differ by <1% from the B3LYP energies, while the average relative stability of V_2 is increased by 0.2 eV (11%).

The local geometries (atomic positions), net Mulliken charges and spin moments of the V_2 and VC=CV defects are shown in Figure 1, where the numerical values refer to the singlet, S_z=0, spin state for the S_{128} cell.

As shown in the lowest part of Figure 1, there is a substantial re-arrangement of the six central atoms of the VC=CV divacancy to give a structure which is not too dissimilar to that of the tetramethyl ethylene molecule, TME $(CH_3)_2C{=}C(CH_3)_2$. Thus, the out-of-plane angle, defined therein as the angle between the A_1, B_1 and B_2 plane and the double bond axis, A_1-A_2, is 23°, while the angles $B_2\widehat{A_1}B_1$ and $B_3\widehat{A_2}B_4$ are 114° and $A_1\widehat{A_2}B_4$ and $A_2\widehat{A_1}B_1$ 120°. Mulliken analyses indicate strong spin localisation at the three atoms nearest neighbours to each vacancy, the most stable of many possible spin distributions leading to local moments of (+0.77 $|e|$, +0.77 $|e|$, -0.56 $|e|$) around one vacancy and moments of the opposite sign around the other, so that the total S_z is zero. The A_1-A_2 and A_1-B_1 (and equivalent) distances of 1.345 Å and 1.521 Å, respectively, are close to electron diffraction values of 1.351 Å and 1.516 Å reported for TME[58], while the double bond distance is also close to that of 1.325 Å, which is calculated for (molecular) ethylene using an identical basis set and functional, whereas the next C-C distances away from the defect essentially coincide with the perfect bulk value of 1.560 Å. The local geometries of the other spin states are close to that of the singlet. On the other hand, as the upper part of Figure 1 shows, in the case of the V_2 divacancy, it is only the local (nn) lattice surrounding the defect that is appreciably perturbed, for the bond distances and tetrahedral angles second neighbour to the vacancies are extremely close to the pure diamond values. For the singlet state, Mulliken analyses indicate again a strong spin localisation at the three atoms nearest neighbours to each vacancy, leading to local moments of (+0.70 $|e|$, +0.70 $|e|$, -0.49 $|e|$) around one vacancy and moments of the oppo-

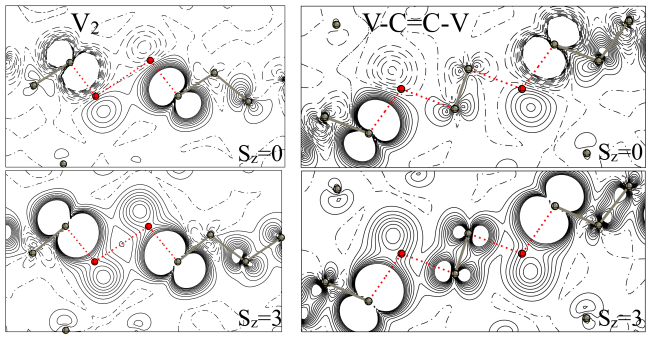

FIG. 2: B3LYP spin density maps of the V_2 and VC=CV defect in diamond for S_z=0 (upper panel) and S_z=3 (lower panel) spin states. Red circles represent the two vacancies while dotted red lines connect the vacancy to its nearest neighbours. Isodensity lines differ by 0.01 $|e|/(a_0)^3$; spin density is truncated at ± 0.1 $|e|/(a_0)^3$. Continuous, dashed and dot-dashed black lines indicate positive, negative and zero values, respectively.

TABLE II: Formation energy (E_f) for V_2 and VC=CV from 6-21G, 6-21G^{opt}, 6-21G*, 6-31 and 6-31* basis sets. Energy differences (δE_f) with respect to 6-21G^{opt} are reported as well. $\Delta E_f = E_f(VC{=}CV) - E_f(V_2)$.

Basis set	V_2		VC=CV		
	E_f	δE_f	E_f	δE_f	ΔE_f
6-21G	9.88	0.06	11.76	-0.09	1.88
6-21G^{opt}	9.94	–	11.67	–	1.73
6-21G*	9.78	0.16	11.48	0.19	1.70
6-31	9.84	0.10	11.56	0.11	1.72
6-31*	9.78	0.16	11.52	0.15	1.74

TABLE III: Formation energy E^f (in eV) for the $S_z = 0$ spin state of the VC=CV, V_2 defects in diamond obtained with HF, various DFT functionals and the S_{64}. [a)] Cluster calculation with the open shell singlet configuration, $C_{190-n}H_{110}$. [b)] Periodic boundary condition supercell calculation with the open shell singlet configuration.

	Method	$E^f_{VC=CV}$	$E^f_{V_2}$	$2{\times}E^f_{V_1}$ [44]
This work	UHF	10.73	8.82	11.92
	B3LYP	11.67	9.94	13.46
	B3LYP+D3	11.83	10.10	14.14
	PBE0	12.47	10.53	14.20
	HSE06	12.37	10.44	13.98
	PBE	11.29	9.40	13.04
	LDA	11.92	9.89	14.02
Ref. 39	BLYP[a]	12.56	10.37	15.24
	PBE[b]	9.21	7.81	12.14

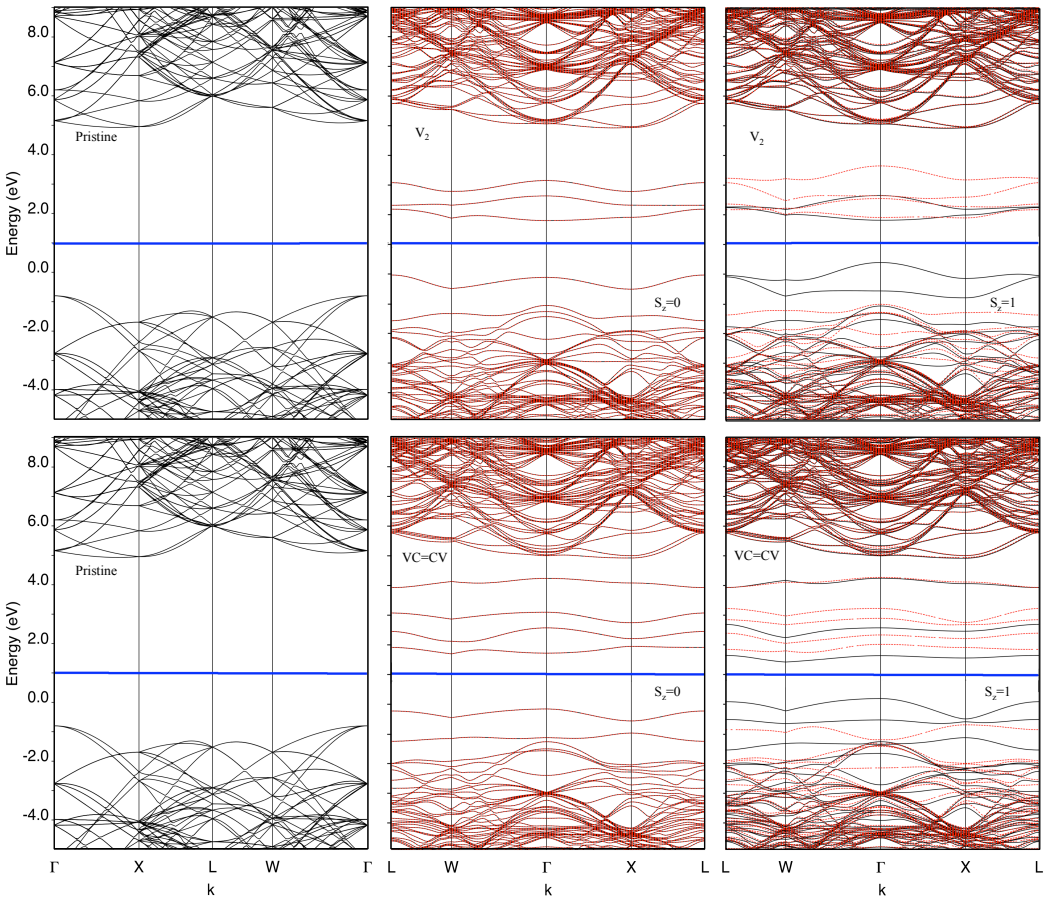

FIG. 3: B3LYP band structures of pristine diamond (1^{st} panel), and the divacancies, V_2 (2^{nd} panel) and VC=CV (3^{rd} panel), based on S_{128} calculations. For the latter two, singlet states are on the left and triplet on the right. Continuous black and dashed red lines indicate α and β bands, respectively. The horizontal blue line represents the Fermi energy.

site sign around the other. Additional points of interest with regard to V_2 are (i) that the degree of spin polarisation increases both with S_z and the percentage of exact exchange in the B3LYP functional, the UHF moments being close to unity; and (ii) that the PBE and LDA moments are extremely small, with a vanishing alternation of the α β spins in the singlet state. Mulliken population analysis, though undoubtedly useful, leads to an arbitrary partition of the electron distribution. A wider, more informative and unbiased description is contained in the charge and spin density maps. Figure 2 shows the singlet and triplet spin densities in planes containing V_2 and VC=CV divacancies and nearest neighbours in a $\langle 111 \rangle$ chain from S_{128} calculations. The maps shown in this Figure provide direct graphical evidence as to reasons why the $\{\alpha\alpha\beta\}$:$\{\alpha\beta\beta\}$ singlet and $\{\alpha\alpha\beta\}$:$\{\alpha\alpha\beta\}$ triplet states (and the reverse spin alignments) are separated by only 2-3 meV, whereas the septet state is 60-80 meV higher in energy.

Turning now to band structures, Figure 3 shows these for pristine diamond, and the singlet and triplet states of V_2 and VC=CV. The most striking, though not unexpected, feature of the divacancy band structures is the reduction in band gap from 5.76 eV to less than 2 eV in all cases. In the singlet states (central panels) the six unpaired/unbound electrons might be expected to occupy three pairs of bands (each α-β pair will result overlapped in the Figure) below the Fermi level, but above the valence bands, and three corresponding unfilled pairs of bands above the Fermi level, E_F, but below the conducting bands. However, for the V_2 divacancy, only 2 α-β pairs are well separated from those of the host lattice, leading to a band gap of 1.91 eV at the Γ-point. In the case of the higher energy VC=CV divacancy, again there are only two pairs of occupied bands that are well separated from the valence bands, but now four empty pairs of bands between E_F and the host conduction bands appear, the fourth being the antibonding level of the double bond between the two vacancies. Here there is a band gap of 1.88 eV at the Γ-point. α and β bands, that are fully degenerate in S_z=0, split in S_z=1 (formally, 4α and 2β) as shown in Figure 3 (right panels), where the split-

ting is more evident in VC=CV than in V_2. For the latter the gap reduces to 1.0 for α electrons, whereas for β electrons it is much larger (2.6 eV). For VC=CV, numbers are similar, nemely 1.1 and 2.2 eV for α and β electrons, respectively.

B. Vibrational properties

Vibrational spectroscopy makes a significant contribution to the identification of the different types of defects present in diamond. While it is generally rather difficult from experiment to assign a given spectral feature unambiguously to a specific structural defect, since, potentially, there are a large number of factors such as defect type, concentration, aggregation etc., that might hinder or complicate this. However, the same is not true for a simulation, since the nature of a particular defect, its concentration and local environment *i.e.*, bulk, surface grain boundary, presence of impurity etc., are defined precisely *a priori*.

The simulated Raman spectra of the singlet spin states of the V_2 and VC=CV divacancy defects in diamond, derived from equilibrium B3LYP lattice structures and energy derivatives at concentrations corresponding to S_{64} and S_{128} supercells, are shown in Figure 4. The first panel contains the spectrum of the pristine host lattice, for comparison, the second and third, those for V_2 and the fourth and fifth, those for VC=CV. The full spectra have been obtained by enveloping each calculated frequency with a pseudo-Voigt function which consists of a linear combination of a Lorentzian and Gaussian functions with full width at half maximum of 8 cm^{-1}. The vertical blue line across the five panels marks the position of the simulated first-order Raman peak of pristine diamond obtained under the same computational conditions as the defective systems: it occurs at 1317 cm^{-1}, 15 cm^{-1} below the experimental peak.

The peak at 1317 cm^{-1} separates the spectra of the defective systems into two regions: at lower wavenumbers there are spectroscopic features due to collective vibrational modes with null intensity in perfect diamond for symmetry reasons. In the defective systems, these features have low relative intensity, and a comparison of the S_{64} and S_{128} spectra indicates that neither divacancy gives rise to specific features in this region of the spectrum. It is a reasonable assumption that peaks above 1317 cm^{-1} in the spectra of defective material that cannot be attributable to any vibrational modes, either inactive for symmetry reasons or with zero intensity, in the spectrum of pristine diamond, are due to defects. The experimental Raman spectrum of defective diamond, reported by Prawer *et al.*[23], shows two major peaks in this region, at 1491 and 1628 cm^{-1}, the origins of which remain a matter of debate. Of various putative attributions, the most widely accepted for the 1628 cm^{-1} is the presence of sp^2 carbon atoms neighbouring the defect. Neither previous calculations for the isolated neutral va-

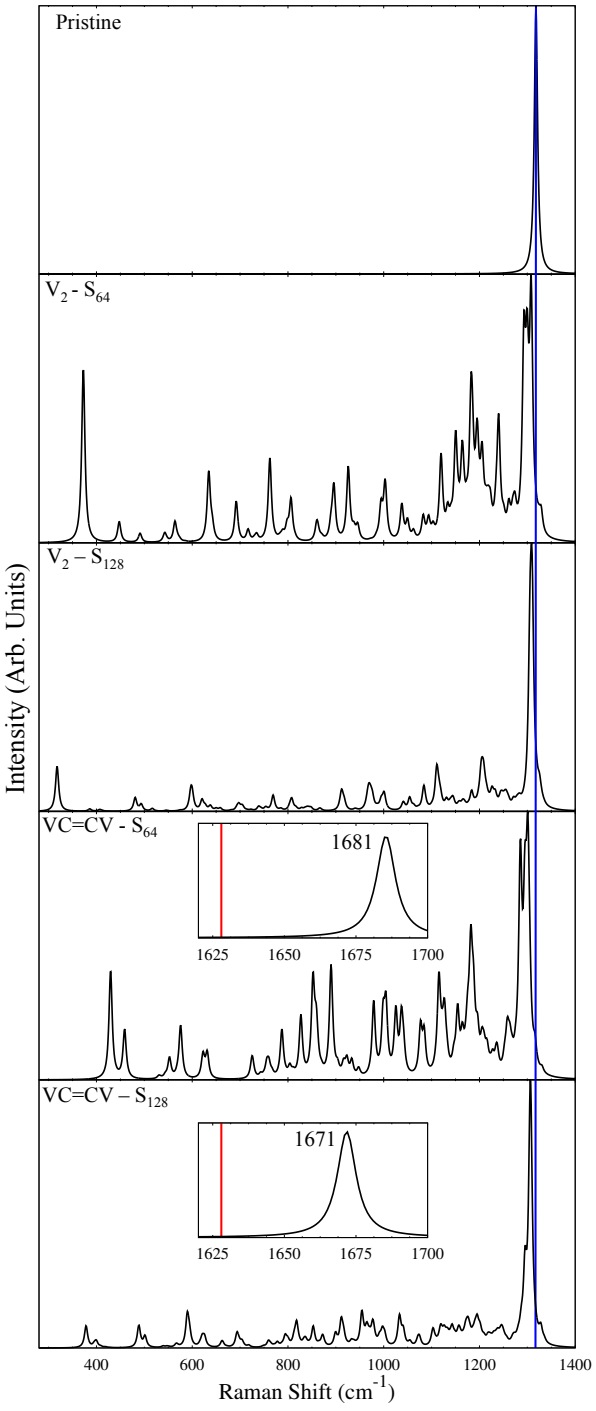

FIG. 4: B3LYP Raman spectra of S_{64} and S_{126} for pristine, V_2 and VC=CV defective structures, the latter two in their most stable singlet spin state. The V_2 spectrum does not show any peak above 1317 cm^{-1}, whereas V-C=C-V presents one peak. The spectral region between 1620 and 1700 cm^{-1} is also reported for this defect in the two boxes, where the vertical red line marks the position of the experimental[23] Raman signal at 1628 cm^{-1}.

cancy in diamond[43], nor the spectrum of the vicinal divacancy shown in Figure 4 exhibit a peak in this region, so that they can be excluded as potential candidates for the two peaks in the experimental spectrum. However, as the fourth and fifth panels of Figure 4 show quite clearly, single peaks occur at 1671 cm^{-1} and 1682 cm^{-1} respectively in the S_{64} and S_{128} spectra of the VC=CV divacancy. The limited dependence of the peak position on defect concentration reported here – the type of information which is notably absent in experimental spectra – suggests that even at lower concentrations the position of this peak is in the range (1650 -1660) cm^{-1}. Animations of the vibrational modes of the VC=CV divacancy (available at `http://www.pmmp.jussieu.fr/yves/defectsindiamond`) yield the contributions of the individual carbon atoms to the collective motion in the defective crystal, and show, specifically, that the 1671 cm^{-1}/1682 cm^{-1} peaks can be attributed to the C=C double bond. It is of interest to note that these values are close the range 1620 – 1680 cm^{-1} that have been reported for (molecular) alkenes.[59] Despite the reduction in intensity of this vibrational mode with decreasing concentration, as is the case with other modes, it remains approximately one quarter that of the first order Raman peak. Finally, the complete absence of intensity in the region of 1491 cm^{-1} in the spectra of both V_2 and VC=CV suggests that this feature of the spectrum reported by Prawer *et al.*[23] is not attributable to either of these divacancies.

IV. CONCLUSIONS

The overall conclusion of this paper is that all-electron B3LYP hybrid calculations within a periodic supercell formulation provide a flexible and reliable approach to the structure, energetics, electronic and spin distributions and vibrational properties of lattice defects in crystalline solids. Specifically, in the case of vacancy defects in diamond the principal conclusions are:

- that the lowest energy states of the isolated neutral vacancy, V_1, and both the vicinal V_2 and VC=CV divacancies, are singlets (S_z=0), followed by the triplet (S_z=1) states;
- that the spin *alignment* in the singlet states of both divacancies is $\{\alpha\alpha\beta\}$:$\{\alpha\beta\beta\}$;
- that V_2 divacancies are more stable than VC=CV for all possible spin configurations, with a difference in energy of ∼1.7 eV for the singlet states;
- that the association, or binding energy of two (isolated) S_z=0 vacancies to form a singlet V_2 is ∼-3.5 eV;
- that the formation energies of 9.9 eV, 11.7 eV and 13.5 eV for V_2, VC=CV and 2×V_1 respectively suggest that their native concentrations in diamond will be extremely small, and that their detectable presence is the result of (external) damage;
- that calculated defect energies from S_{64} and S_{128} supercells are effectively indistinguishable;
- that the use of richer basis sets than Pople's 6-21G leads to no meaningful differences in energy;
- that other hybrid functionals and one-electron approximations predict an identical pattern of stability with regard to V_2 and VC=CV;
- that the calculated first-order Raman peak in pristine diamond, 1317 cm^{-1}, is within 1% of the measured value, which gives weight to the description of the defective systems;
- that there is a small shift of 10-13 cm^{-1} of the first-order peak in the defective systems, which suggests that the perturbation of the lattice beyond the immediate vicinity of the divacancies is minimal;
- that neither divacancy gives rise to specific spectral features below the first-order peak;
- that the peak at 1671/1681 cm^{-1} in the spectrum of the VC=CV defective system, which is associated with the C=C double bond, is a candidate for the 1628 cm^{-1} peak reported by Prawer *et al.*[23]

[1] C. A. Coulson and M. J. Kearsley. Colour Centres in Irradiated Diamonds. I. *Proc. R. Soc. A*, 241(1227):433–454, 1957.

[2] R. P. Messmer and G. D. Watkins. Molecular-Orbital Treatment for Deep Levels in Semiconductors: Substitutional Nitrogen and the Lattice Vacancy in Diamond. *Phys. Rev. B*, 7:2568–2590, 1973.

[3] A. Mainwood and A. M. Stoneham. Stability of Electronic States of the Vacancy in Diamond. *Journal of Physics: Condensed Matters*, 9(11):2453, 1997.

[4] S. J. Breuer and P. R. Briddon. *Ab initio* Investigation of the Native Defects in Diamond and Self-Diffusion. *Phys. Rev. B*, 51(11):6984, 1995.

[5] J. P. Goss, B. J. Coomer, R. Jones, C. J. Fall, P. R. Briddon, and S. Öberg. Extended Defects in Diamond: The Interstitial Platelet. *Phys. Rev. B*, 67:165208, Apr 2003.

[6] G. B. B. M. Sutherland, D. E. Blackwell, and W. G. Simeral. The Problem of the Two Types of Diamond. *Nature*, 174:901–904, 1954.

[7] J. A. van Wyk, O. D. Tucker, M. E. Newton, J. M. Baker, G. S. Woods, and P. Spear. Magnetic-Resonance Measurements on the $^5A_2$ Excited State of the Neutral Vacancy in Diamond. *Phys. Rev. B*, 52:12657–12667, 1995.

[8] G. Davies, S. C. Lawson, A. T. Collins, A. Mainwood, and

S. J. Sharp. Vacancy-Related Centers in Diamond. *Phys. Rev. B*, 46:13157–13170, 1992.

[9] J. Isoya, H. Kanda, Y. Uchida, S. C. Lawson, S. Yamasaki, H. Itoh, and Y. Morita. EPR Identification of the Negatively Charged Vacancy in Diamond. *Phys. Rev. B*, 45:1436–1439, 1992.

[10] R. B. Jackman. Special issue: Diamond Electronics-Preface. *Semicond. Sci. Technol.*, 18(3):1–2, 2003.

[11] R. J. Nemanich, J. A. Carlisle, A. Hirata, and K. Haenen. CVD Diamond - Research, Applications, and Challenges. *MRS Bull.*, 39(06):490–494, 2014.

[12] A. Hoffman, S. Prawer, and R. Kalish. Structural Transformation of Diamond Induced by 1-keV Ar-Ion Irradiation as Studied by Auger and Secondary-Electron Spectroscopies and Total-Secondary-Electron-Yield Measurements. *Phys. Rev. B*, 45(22):12736, 1992.

[13] S. Lagomarsino, P. Olivero, S. Calusi, D. Gatto Monticone, L. Giuntini, M. Massi, S. Sciortino, A. Sytchkova, A. Sordini, and M. Vannoni. Complex Refractive Index Variation in Proton-Damaged Diamond. *Opt. Express*, 20(17):19382–19394, 2012.

[14] J. F. Prins. Onset of Hopping Conduction in Carbon-Ion-Implanted Diamond. *Phys. Rev. B*, 31(4):2472, 1985.

[15] R. Kalish, A. Reznik, S. Prawer, D. Saada, and J. Adler. Ion-Implantation-Induced Defects in Diamond and Their Annealing: Experiment and Simulation. *Phys Status Solidi (a)*, 174(1):83–99, 1999.

[16] R. Kalish, A. Reznik, K. W. Nugent, and S. Prawer. The Nature of Damage in Ion-Implanted and Annealed Diamond. *Nucl. Instr. Meth. Phys. Res. B*, 148(1):626–633, 1999.

[17] D. J. Twitchen, D. C. Hunt, M. E. Newton, J. M. Baker, T. R. Anthony, and W. F. Banholzer. Electron Paramagnetic Resonance (EPR) and Optical Absorption Studies of Defects Created in Diamond by Electron Irradiation Damage at 100 and 350K. *Physica B: Condensed Matter*, 273:628–631, 1999.

[18] P. F. Lai, S. Prawer, and C. Noble. Electron Spin Resonance Investigation of Ion-Irradiated Diamond. *Diamond Relat. Mater.*, 11(7):1391–1396, 2002.

[19] A. Moroño, S. M. G. de Vicente, and E. R. Hodgson. Radiation Effects on the Optical and Electrical Properties of CVD Diamond. *Fusion. Eng. Des.*, 82(15):2563–2566, 2007.

[20] H. Amekura and N. Kishimoto. Effects of High-Fluence Ion Implantation on Colorless Diamond Self-Standing Films. *J. Appl. Phys.*, 104(6):63509, 2008.

[21] D. N. Jamieson, S. Prawer, K. W. Nugent, and S. P. Dooley. Cross-Sectional Raman Microscopy of MeV Implanted Diamond. *Nucl. Instrum. Methods Phys. Rese. B*, 106(1):641–645, 1995.

[22] J. D. Hunn, S. P. Withrow, C. W. White, and D. M. Hembree Jr. Raman Scattering from MeV-Ion Implanted Diamond. *Phys. Rev. B*, 52(11):8106, 1995.

[23] S. Prawer, K. W. Nugent, and D. N. Jamieson. The raman spectrum of amorphous diamond. *Diamond Relat. Mater.*, 7(1):106–110, 1998.

[24] J. O. Orwa, K. W. Nugent, D. N. Jamieson, and S. Prawer. Raman Investigation of Damage Caused by Deep Ion Implantation in Diamond. *Phys. Rev. B*, 62(9):5461, 2000.

[25] R. Brunetto, G. A. Baratta, and G. Strazzulla. Raman Spectroscopy of Ion Irradiated Diamond. *J. Appl. Phys.*, 96(1):380–386, 2004.

[26] P. Olivero, S. Rubanov, P. Reichart, B. C. Gibson, S. T. Huntington, J. R. Rabeau, Andrew D. Greentree, J. Salzman, D. Moore, D. N. Jamieson, and S. Prawer. Characterization of Three-Dimensional Microstructures in Single-Crystal Diamond. *Diamond Relat. Mater.*, 15(10):1614–1621, 2006.

[27] S. Prawer, I. Rosenblum, J. O. Orwa, and J. Adler. Identification of the Point Defects in Diamond as Measured by Raman Spectroscopy: Comparison Between Wxperiment and Computation. *Chem. Phys. Lett.*, 390(4):458–461, 2004.

[28] A. A. Bergman, A. M. Zaitsev, M. Huang, and A. A. Gorokhovsky. Photoluminescence and Raman Studies of Xe Ion-Implanted Diamonds: Dependence on Implantation Dose. *J. Lumin.*, 129(12):1524–1526, 2009.

[29] C. Kittel. *Introduction to Solid State*. John Wiley & Sons, 1966.

[30] G. S. Woods. Infrared Absorption Studies of the Annealing of Irradiated Diamonds. *Philos. Mag. B*, 50(6):673–688, 1984.

[31] P. J. Lin-Chung. Local Vibrational Modes of Impurities in Diamond. *Phys. Rev. B*, 50(23):16905, 1994.

[32] R. Dovesi, R. Orlando, A. Erba, C. M. Zicovich-Wilson, B. Civalleri, S. Casassa, L. Maschio, M. Ferrabone, M. De La Pierre, P. D'Arco, Y. Noël, M. Causà, M. Rérat, and B. Kirtman. CRYSTAL14: A Program for the *Ab Initio* Investigation of Crystalline Solids. *Int. J. Quantum Chem.*, 114:1287, 2014.

[33] L. Maschio, B. Kirtman, R. Orlando, and M. Rérat. *Ab Initio* Analytical Infrared Intensities for Periodic Systems Through a Coupled Perturbed Hartree-Fock/Kohn-Sham Method. *J. Chem. Phys.*, 137(20):204113, 2012.

[34] L. Maschio, B. Kirtman, M. Rérat, R. Orlando, and R. Dovesi. *Ab initio* Analytical Raman Intensities for Periodic Systems Through a Coupled Perturbed Hartree-Fock/Kohn-Sham Method in an Atomic Orbital Basis. I. Theory. *J. Chem. Phys*, 139(16):164101, 2013.

[35] L. Maschio, B. Kirtman, M. Rérat, R. Orlando, and R. Dovesi. *Ab initio* Analytical Raman Intensities for Periodic Systems Through a Coupled Perturbed Hartree-Fock/Kohn-Sham Method in an Atomic Orbital Basis. II. Validation and Comparison with Experiments. *J. Chem. Phys*, 139(16):164102, 2013.

[36] C. Carteret, M. De La Pierre, M. Dossot, F. Pascale, A. Erba, and R. Dovesi. The Vibrational Spectrum of $CaCO_3$ Aragonite: a Combined Experimental and Quantum-Mechanical Investigation. *J. Chem. Phys.*, 138(1):014201, 2013.

[37] L. Maschio, B. Kirtman, S. Salustro, C. M. Zicovich-Wilson, R. Orlando, and R. Dovesi. Raman Spectrum of Pyrope Garnet. A Quantum Mechanical Simulation of Frequencies, Intensities, and Isotope Shifts. *J. Phys. Chem. A*, 117(45):11464–11471, 2013.

[38] M. Prencipe, L. Maschio, B. Kirtman, S. Salustro, A. Erba, and R. Dovesi. Raman Spectrum of $NaAlSi_2O_6$ Jadeite. A Quantum Mechanical Simulation. *J. Raman Spectrosc.*, 45:703–709, 2014.

[39] D. Hyde-Volpe, B. Slepetz, and M. Kertesz. The [V−C=C−V] Divacancy and the Interstitial Defect in Diamond: Vibrational Properties. *J. Phys. Chem. C*, 114(21):9563–9567, 2010.

[40] A. D. Becke. Density-Functional Thermochemistry. III. The Role of Exact Exchange. *J. Chem. Phys.*, 98(7):5648–5652, 1993.

[41] C. Lee, W. Yang, and R. G. Parr. Development of the Colle-Salvetti Correlation-Energy Formula Into a Func-

tional of the Electron Density. *Phys. Rev. B*, 37(2):785, 1988.

[42] M. De La Pierre, R. Orlando, L. Maschio, K. Doll, P. Ugliengo, and R. Dovesi. Performance of Six Functionals (LDA, PBE, PBESOL, B3LYP, PBE0, and WC1LYP) in the Simulation of Vibrational and Dielectric Properties of Crystalline Compounds. The Case of Forsterite Mg_2SiO_4. *J. Comput. Chem.*, 32(9):1775–1784, 2011.

[43] J. Baima, A. Zelferino, P. Olivero, A. Erba, and R. Dovesi. Raman Spectroscopic Features of the Neutral Vacancy in Diamond from *Ab Initio* Quantum-mechanical Calculations. *Phys. Chem. Chem. Phys.*, 18(3):1961–1968, 2015.

[44] A. Zelferino, S. Salustro, J. Baima, V. Lacivita, R. Orlando, and R. Dovesi. The Electronic States of the Neutral Vacancy in Diamond: a Quantum Mechanical Approach. *Theor. Chem. Acc.*, 135(3):1–11, 2016.

[45] S. Salustro, A. Erba, C. M. Zicovich-Wilson, Y. Nöel, L. Maschio, and R. Dovesi. Infrared and Raman Spectroscopic Features of the Self-Interstitial Defect in Diamond from Exact-Exchange Hybrid DFT Calculations. *Phys. Chem. Chem. Phys.*, 120:21288–21295, 2016.

[46] S. Salustro, Y. Nöel, C. M. Zicovich-Wilson, P. Olivero, and R. Dovesi. The V+I Defects in Diamond: an *Ab Initio* Investigation of the Electronic Structure, of the Raman and IR Spectra, and of their Possible Recombination . *J. Chem. Phys.*, 145(18):184701, 2016.

[47] S. Salustro, A. Ferrari, R. Orlando, and R. Dovesi. Comparison Between Cluster and Supercell Approaches: The Case of Defects in Diamond. *Theor. Chem. Acc.*, 135(3), 2016.

[48] C. Adamo and V. Barone. Toward Chemical Accuracy in the Computation of NMR Shieldings: the PBE0 Model. *Chem. Phys. Lett.*, 298(1):113–119, 1998.

[49] A. V. Krukau, O. A. Vydrov, A. F. Izmaylov, and G. E. Scuseria. Influence of the Exchange Screening Parameter on the Performance of Screened Hybrid Functionals. *J. Chem. Phys.*, 125(22):224106–224106, 2006.

[50] S. Grimme, J. Antony, S. Ehrlich, and H. Krieg. A Consistent and Accurate *Ab Initio* Parametrization of Density Functional Dispersion Correction (DFT-D) for the 94 Elements H-Pu. *J. Chem. Phys.*, 132:154104, 2010.

[51] J. S. Binkley, J. A. Pople, and W. J. Hehre. Self-Consistent Molecular Orbital Methods. 21. Small Split-Valence Basis Sets for First-Row Elements. *J. Am. Chem. Soc.*, 102(3):939–947, 1980.

[52] M. M. Francl, W. J. Petro, W. J. Hehre, J. S. Binkley, M. S. Gordon, D. J. DeFrees, and J. A. Pople. Self-Consistent Molecular Orbital Methods. XXIII. A Polarization-Type Basis Set for Second-Row Elements. *J. Chem. Phys.*, 77(7):3654–3665, 1982.

[53] J. P. Perdew, K. Burke, and M. Ernzerhof. Generalized Gradient Approximation Made Simple. *Phys. Rev. Lett.*, 77(18):3865–3868, 1996.

[54] P. A. M. Dirac. A Theory of Electrons and Protons. *Proc. R. Soc. A*, 126(801):360–365, 1930.

[55] H. J. Monkhorst and J. D. Pack. Special Points for Brillouin-Zone Integrations. *Phys. Rev. B*, 13(12):5188, 1976.

[56] F. Pascale, C. M. Zicovich-Wilson, F. Lòpez Gejo, B. Civalleri, R. Orlando, and R. Dovesi. The Calculation of the Vibrational Frequencies of the Crystalline Compounds and its Implementation in the CRYSTAL Code. *J. Comput. Chem.*, 25(6):888–897, 2004.

[57] C. M. Zicovich-Wilson, F. Pascale, C. Roetti, V. R. Saunders, R. Orlando, and R. Dovesi. Calculation of the Vibration Frequencies of α-Quartz: The Effect of Hamiltonian and Basis Set. *J. Comput. Chem.*, 25(15):1873–1881, 2004.

[58] J. L. Carlos and S. H. Bauer. Gas Phase Structure of Tetramethylethylene. *Journal of the Chemical Society, Faraday Transactions 2: Molecular and Chemical Physics*, 70:171–176, 1974.

[59] R. M. Silverstein, G. C. Bassler, and T. C. Morrill. *Spectrometric Identifications of Organic Compounds*. John Wiley & Son, 1998.